ChemCatChem

Supporting Information

Influence of the Ageing and Drying Steps of a CoMoP/γ-Al_2O_3 Catalyst onto the Multi-Scale Molybdenum Active Phase Organization

Candice Cottrez, Séverine Humbert, Anne-Sophie Gay,* Elodie Devers, Frédéric De Geuser, Xavier Carrier, and Alexandra Chaumonnot

Theoretical Aspects of ASAXS

Considering a homogeneous matrix including randomly oriented particles with identical shape and with size parameterized by R, the SAXS scattered intensity is defined by:

$$I(q) = \frac{N_p}{V_s}\,\Delta\rho^2 \int_0^\infty P(R)V(R)^2|F(q,R)|^2\Psi(q,R)\mathrm{d}R \qquad (1)$$

where N_p the number of particles, V_s the sample volume, $P(R)$ the size distribution function, $F(q,R)$ the form factor, $\Psi(q,R)$ the structure factor which equals to 1 when the particles are well spaced, *i.e.* when distances between particles are larger than particle sizes, and $\Delta\rho^2$ the contrast factor such as:

$$\Delta\rho^2 = \left(\rho_p - \rho_m\right)^2 \qquad (2)$$

ρ_p and ρ_m the scattering length densities of the particles and the matrix:

$$\rho = r_e \sum_j n_j f_j \qquad (3)$$

n_j the number density of the atom j in the matrix or in the particles, f_j the atomic form factors and r_e the classical Thomson radius (r_e = 0.282 10^{-12} cm).

As the system studied here is composed of metal particles supported on a porous support such as alumina, the latter, and particularly its pores, will contribute significantly to the SAXS signal, making it impossible to distinguish the nanoparticles. Therefore, it is mandatory to record the SAXS signal at different incident beam energies close to the metal absorption edge. In that way, it is possible to isolate the specific signals of each phase. Since the Mo arrangement looks to be described here, measurements will be carried out close to the Mo K-edge absorption.

It is recalled that the atomic form factor of a species j can be written:

$$f_j(E) = f_0 + f_j'(E) + i f_j''(E) \quad (4)$$

with $f_0 = Z$, the atomic number.

Atomic diffusion factor $f_j'(E)$ and $f_j''(E)$ close to the Mo K-edge absorption (at 20000 eV) are reported in Table 1.

Table 1. Atomic diffusion factor $f_j'(E)$ and $f_j''(E)$ [1,2] close to the Mo K-edge absorption

	Energy (eV)	$f_j'(E)$	$f_j''(E)$
E_5	19990	-6,941	0,638
E_4	19975	-5,980	0,554
E_3	19940	-5,096	0,542
E_2	19860	-4,264	0,544
E_1	19700	-3,538	0,551

The subtraction method developed by Haubold *et al.* [3,4,5,6,7] has been adapted here to extract the ASAXS signal from metal particles. It consists in subtracting the intensities measured at two different energies and using the resulting intensity as a function of the particle scattering.

Subtraction method

As the system here is composed of particles p supported on a porous support s and with pores filled by air, the scattered intensity can be defined thanks to the partial structure factors S_{pp}, S_{ss} and S_{sp} described by Binninger *et al.* [8] as follows:

$$\langle I(q,E)\rangle = |f_s|^2 n_s^2 r_e^2 S_{ss}(q) + 2\Re\left(f_p(E) f_s^*\right) n_p n_s\, r_e^2 S_{sp}(q) + \left|f_p(E)\right|^2 n_p^2 r_e^2 S_{pp}(q) \quad (5)$$

with $\Re$ the real part and $*$ the complex conjugate.

The electronic density of the porous support and the particles $\sum_j n_j f_j$ is simplified by the terms $n_s f_s$ and $n_p f_p$ respectively to lighten the writing and be coherent with literature notation on this subject .

The main advantage of acquiring the scattered intensity at different energies is that the scattering length density of the metal particle is varied without varying the one of the porous support. Thus, the contribution of the mesoporous support $S_{ss}(q)$ is suppressed. However, the contribution from the metal-support interference $S_{sp}(q)$ remains to be considered. Moreover, neglecting the imaginary parts of f_s and f_p, the difference between the intensities measured at two different energies E_i and E_j permits to express the equation (5) as:

$$\langle I(q,E_i)\rangle - \langle I\left(q,E_j\right)\rangle = n_p^2 r_e^2 \left(\left|f_p(E_i)\right|^2 - \left|f_p\left(E_j\right)\right|^2\right).\left(S_{pp}(q) + \alpha S_{sp}(q)\right) \quad (6)$$

where $\alpha = \frac{n_s f_s}{n_p \overline{f_p}}$ and $\overline{f_p} = \frac{f_p(E_i)+f_p(E_j)}{2}$ is the mean value of $f_p(E)$.

Considering independent spherical metallic particles of radius R_p deposited on a spherical support particle of radius R_s, it is possible to write $S_{pp}(q)$, and $S_{sp}(q)$ as follows:

$$S_{pp}(q) = \frac{N_p}{V_s} \int_0^{+\infty} P_p(R_p) V_p^2(R_p)\, F_p^2(q, R_p) dR_p \tag{7}$$

$$S_{sp}(q) = \frac{N_p}{V_s} \iint_0^{\infty} P_p(R_p) P_s(R_s) V_p(R_p) V_s(R_s) F_p(q, R_p) F_s(q, R_s) \frac{sin\left(q(R_p + R_s)\right)}{q(R_p + R_s)} \, \mathrm{d}R_p \mathrm{d}R_s \tag{8}$$

In the present case, $\alpha \sim 0.83$ so the interference term S_{sp} is maybe not negligible. Both terms will be considered the data modeling.

An example of ASAXS $I(E_3) - I(E_5)$ curves obtained by the subtraction method for the 26_A_D catalyst is represented in Figure 1.

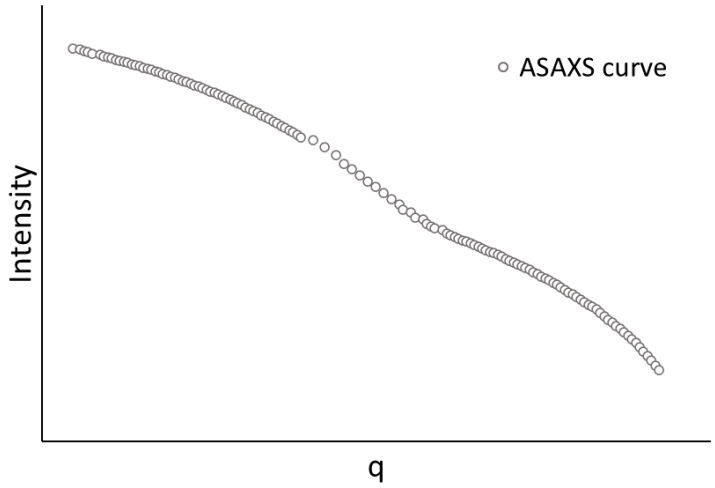

Figure 1. ASAXS curves ($I(E_3) - I(E_5)$) obtained by the subtraction method for the 26_A_D catalyst

ASAXS data modeling

To evaluate the size distribution of the sulfided slabs, a nonlinear least-squares adjustment of the ASAXS signal is performed on equation (6). The assumptions made for the choice of the regression model are listed below.

ASAXS $I(E_3) - I(E_5)$ curves show two inflections of the scattered signal as seen in Figure 1. Consequently, two types of molybdenum objects must be considered. These two populations are attributed to isolated slab at a smaller scale and moderately dense slab aggregates at a larger scale, thanks to electron microscopy observations. Thus, we consider that scattering objects can be porous. The porosity is named ε. In the case of crystalline slabs, ε = 0 and in the case of slab aggregates, ε > 0.

The number of molybdenum atoms in the scattering object is expressed as[9]:

$$N_{Mox} = \frac{N_A \times \rho_{Mox}}{M_{Mox}} \times V \times (1 - \varepsilon) \quad (9)$$

where M_{Mox} = MoS_2 in the case of sulfided molybdenum and M_{Mox} = MoO_y in the case of oxide molybdenum, V the volume of the scattering object, N_A the Avogadro's number (6.022×10^{23} mol^{-1}), M_{Mox} the molar mass in g/mol and ρ_{Mox} the density (g/cm^3) of the molybdenum phase.

Hence, the scattering factor of a molybdenum object is defined by:

$$n_p f_p = \left(\frac{N_A \times \rho_{Mox}}{M_{Mox}} \times f_{Mox}\right) \times (1 - \varepsilon) \quad (10)$$

Thus, the term $\frac{N_p}{V_s}$ from the equation (1) can be written as:

$$\frac{N_p}{V_s} = \frac{w_{Mox} \times \rho_s}{\rho_{Mox}} \times \frac{1}{1 - \varepsilon} \times \frac{1}{\langle V \rangle} \quad (11)$$

with $\langle V \rangle$ the mean volume of the slab stack or slab aggregate (cm^{-3}), w_{Mox} the weight concentration of the molybdenum phase (wt%), ρ_s the sample structural density (g/cm^3).

Isolated and stacked slabs can be modelled as discs of height $2H$ and radius R_p. The corresponding form factor is:

$$F_{disc}^2(q, R_p, H) = 4 \int_0^{\pi/2} \left(\frac{\sin^2(qH\cos\beta)}{(qH)^2 \cos^2\beta}\right) \frac{J_1^2(qR_p \sin\beta)}{(qR_p)^2 \sin^2\beta} \sin\beta \, d\beta \quad (12)$$

and

$$V_p(R_p, H) = \pi {R_p}^2 2H \quad (13)$$

As for the slab aggregates, they can be modelled as an ellipsoid of axes (R_a, R_a, and νR_a), the used shape factor is then the following:

$$F_{ellipsoid}^2(q, R_a, \nu) = \int_0^1 \Phi^2 \left[qR_a\left(1 + x^2(\nu^2 - 1)\right)^{0.5}\right] dx \quad (14)$$

with

$$\Phi(t) = 3\left(\frac{\sin t - t\cos t}{t^3}\right) \quad (15)$$

and

$$V_a(R_a, \nu) = \frac{4}{3}\pi\nu {R_a}^3 \quad (16)$$

The size distributions of isolated/stacked slabs and slab aggregates are modelled by the lognormal distribution such as:

$$P_k(R_k) = \frac{1}{\sqrt{2\pi}R_k\sigma_k}\exp\left(-\frac{(\ln R_k - \mu_k)^2}{2\sigma_k^2}\right) \quad (17)$$

where k is equal to p for isolated/stacked slabs and equal to a for slab aggregates, and μ and σ are the scale and shape parameters of the lognormal distribution, respectively.

To calculate the number, surface and volume average sizes from the adjusted lognormal distribution, the distributions moments M_{n} must be known:

$$M_{n_k} = \exp\left(\mu_k \times n + \frac{n^2{\sigma_k}^2}{2}\right) \quad (18)$$

Thus, the average size of the isolated/stacked slabs in number and volume can be calculated, as well as for the slab aggregates:

$$Rp_{num} = \frac{M_{1_p}}{M_{0_p}} = \exp\left(\mu_p + \frac{\sigma_p^2}{2}\right) \text{ and } Rp_{vol} = \frac{M_{3_p}}{M_{2_p}} = \exp\left(\mu_p + \frac{5\sigma_p^2}{2}\right) \quad (19)$$

$$Ra_{num} = \frac{M_{1_a}}{M_{0_a}} = \exp\left(\mu_a + \frac{\sigma_a^2}{2}\right) \text{ and } Ra_{vol} = \frac{M_{4_a}}{M_{3_a}} = \exp\left(\mu_a + \frac{7\sigma_a^2}{2}\right) \quad (20)$$

It is now possible to write the term $S_{pp}(q)$ in equation (7) such as:

$$S_{pp}(q) = \left[\frac{N_{pp}}{V_s}\int_0^{+\infty} P_p(R_p)\ V_p^2(R_p, H)F_{disc}^2(q, R_p, H)dR_p + \frac{N_{pa}}{V_s}\int_0^{+\infty} P_a(R_a)V_a^2(R_a, \nu)F_{ellipsoid}^2(q, R_a, \nu)\,dR_a\right] \quad (21)$$

with

$$\frac{N_{pp}}{V_s} = \frac{w_{Mox} \times \rho_s}{\rho_{Mox}} \times w_p \times \frac{1}{1-\varepsilon_p} \times \frac{1}{\langle V_p\rangle} \quad (22)$$

and

$$\frac{N_{pa}}{V_s} = \frac{w_{Mox} \times \rho_s}{\rho_{Mox}} \times w_a \times \frac{1}{1-\varepsilon_a} \times \frac{1}{\langle V_a\rangle} \quad (23)$$

where w_p and w_a are the fraction of molybdenum involved in the isolated/stacked slabs or slab aggregates, respectively, and $\langle V_p\rangle$ and $\langle V_a\rangle$ are the mean volumes of the isolated/stacked slabs and slab aggregates, such as:

$$\langle V_p\rangle = \pi \times 2H \times \int {R_p}^2 P_p(R_p)\mathrm{d}R_p = \pi \times M_{2_p} \times 2H = \pi \times 2H \times \exp\left(2\mu_p + \frac{4\sigma_p^2}{2}\right) \quad (24)$$

$$\langle V_a\rangle = \frac{4}{3} \times \pi \times \nu \times \int {R_a}^3 P_a(R_a)\mathrm{d}R_a = \frac{4}{3} \times \pi \times \nu \times M_{3_a} = \frac{4}{3} \times \pi \times \nu \times \exp\left(3\mu_a + \frac{9\sigma_a^2}{2}\right) \quad (25)$$

Interference between support and molybdenum phase

The interference between the alumina support and molybdenum phase $S_{sp}(q)$ described in equation (8) must be considered. Therefore, the size distribution $P_s(R_s)$, the particle volume $V_s(R_s)$ and the form factor $F(q, R_s)$ must be defined. Pure alumina support has been analyzed by SAXS to determine these different terms. The support structure can be described by:

$$F_s(q, R_s) = 3\left(\frac{\sin qR_s - qR_s \cos qR_s}{(qR_s)^3}\right) \tag{26}$$

and

$$V_s(R_s) = \frac{4}{3}\pi {R_s}^3 \tag{27}$$

and with a bimodal lognormal distribution such as:

$$P_s(R_s) = \frac{1}{\mathrm{C}_1 + \mathrm{C}_2}\left(\mathrm{C}_1 \times P_{s1}(R_s) + \mathrm{C}_2 \times P_{s2}(R_s)\right) \tag{28}$$

with $\mathrm{C}_1 = 1$, $\mathrm{C}_2 = 0.21$, μ_{s1} = 2.88, σ_{s1} = 0.33, μ_{s2} = 2.74 and σ_{s2} = 0.69.

Final model

Finally, considering the first population of Mo particles as isolated/stacked slabs and the second one as aggregates of partially dense slabs, it is possible to write the equation (6) such as:

$$\langle I(q, E_i)\rangle - \langle I\left(q, E_j\right)\rangle = w_{\mathrm{Mo_x}} \times w_p \times \frac{\rho_s}{\rho_{\mathrm{Mo_x}}} \times \Delta^2_{\mathrm{Mo_x}}\left(E_i, E_j\right) \times \left(S'_{pp} + \alpha S'_{sp}\right) \tag{29}$$

with

$$\Delta^2_{\mathrm{Mo_x}}\left(E_i, E_j\right) = {r_e}^2 \times \left[\left(n_{\mathrm{Mo_x}} f_{\mathrm{Mo_x}}(E_i)\right)^2 - \left(n_{\mathrm{Mo_x}} f_{\mathrm{Mo_x}}\left(E_j\right)\right)^2\right] \tag{30}$$

$$S'_{pp}(q) = \left[\frac{1}{< V_p >}\int_0^{+\infty} P_p\left(R_p\right)\, V_p^2\left(R_p, H\right) F^2_{disc}\left(q, R_p, H\right) \mathrm{d}R_p + \frac{w_a(1-\varepsilon_a)}{w_p} \times \frac{1}{< V_a >}\int_0^{+\infty} P_a(R_a) V_a^2(R_a, \nu) F^2_{ellipsoid}(q, R_a, \nu)\, \mathrm{d}R_a\right] \tag{31}$$

$$S'_{sp}(q) = \left[\frac{1}{< V_p >}\iint_0^{\infty} P_s(R_s) V_s(R_s) F_s(q, R_s) P_p\left(R_p\right) V_p\left(R_p, H\right) F_{disc}\left(q, R_p, H\right) \frac{\sin\left(q\left(R_p + R_s\right)\right)}{q\left(R_p + R_s\right)} dR_p dR_s + \frac{w_a(1-\varepsilon_a)}{w_p} \times \frac{1}{< V_a >}\iint_0^{\infty} P_s(R_s) V_s(R_s) F_s(q, R_s) P_a(R_a) V_a(R_a, \nu) F_{ellipsoid}(q, R_a, \nu) \frac{sin\left(q(R_a + R_s)\right)}{q(R_a + R_s)} dR_a dR_s\right] \tag{32}$$

Obtained parameters

As explained earlier, the model estimates the isolated/stacked slabs size distribution (μ_p, σ_p) and the slab aggregate size distribution (μ_a, σ_a). Thus, several average object sizes can be calculated in number, surface or volume.

Thus, the isolates/stacked slabs size distributions (μ_p, σ_p), the slab aggregates size distributions (μ_a, σ_a), and the parameter $\frac{w_a(1-\varepsilon_a)}{w_p}$ allow us to extract much information.

Isolated/stacked slabs scale

Several parameters can be estimated to describe the isolated/stacked slabs, but only two are of special interest:

- the mean slab length L_{slabs} (in number), such as:

$$L_{slabs} = 2 \times R_p \tag{33}$$

- the average stacking S_{slabs}, such as:

$$S_{slabs} = 0.5 \times \frac{2H}{3.1} + 0.5 \tag{34}$$

3.1 Å is the thickness of a slab according to crystallography. The number averaged length is considered here so that it could be easily compared to the mean length measured in TEM.

Slab aggregates scale

Several parameters can describe the slab aggregates, as followed:

- the mean aggregate width W_{ag} (in volume), such as:

$$W_{ag} = 2 \times R_a \tag{35}$$

- the relative Mo amount (in%) involved in the slab aggregates C_{ag}, such as:

$$C_{ag} = \frac{w\mathfrak{E}}{1+w\mathfrak{E}} \times 100 \text{ and } w\mathfrak{E} = \frac{w_a(1-\varepsilon_a)}{w_p} \tag{36}$$

- the absolute Mo amount (in%) involved in the slab aggregates $Absolute\ C_{ag}$, such as:

$$Absolute\ C_{ag} = C_{ag} \times w_{\mathrm{Mo_x}} \tag{37}$$

- the mean volume of slab aggregates $\langle V_{ag} \rangle$ (in nm^3), such as:

$$\langle V_{ag} \rangle = \frac{4}{3} \times \pi \times exp\left(3\mu_a + \frac{9\sigma_a^2}{2}\right) \times \nu \tag{38}$$

- the aggregate number density $\frac{N_{ag}}{V_s}$, such as:

$$\frac{N_{ag}}{V_s} = \frac{w_{\mathrm{Mo_x}} \times \rho_s}{\rho_{\mathrm{Mo_x}}} \times w_{ag} \frac{1}{1-\varepsilon} \times \frac{1}{\langle V_{ag} \rangle} \quad (39)$$

where ρ_s the structural density of the sample here is around 1.31, 1.40, 1.57 and 1.72 g/cm^3 for the 18, 22, 36 and 30 wt% MoO_3 catalysts respectively.

Example of fit

An example of fit is presented in Figure 2 for the 26_A_D sample. The first part of the curve (from 10^{-1} Å^{-1} to 1 Å^{-1}) is essentially due to the contribution of the first population of isolated/stacked slabs whereas the second part of the curve (from 10^{-2} Å^{-1} to 10^{-1} Å^{-1}) is due to the contribution of the second population of larger objects attributed as slab aggregates.

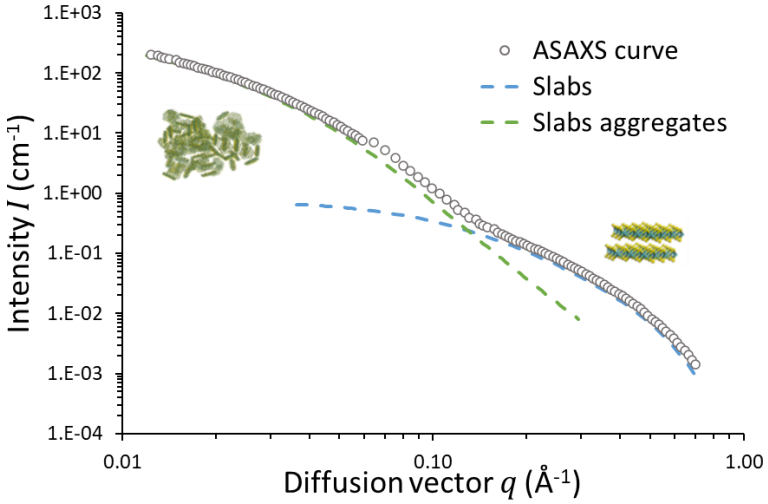

Figure 2. ASAXS curves ($I(E_3) - I(E_5)$) obtained by the subtraction method for the 26_A_D catalyst and fit of the experimental ASAXS data

Standard errors evaluation

Since ASAXS is an unusual technique based on log normal representations and morphological models, ASAXS measurements have been performed on the same sample (*i.e.* 26_A_D) at a single and exact same point to estimate the intrinsic standard error of the technique. Thus, the three ASAXS $I(E_3) - I(E_5)$ curves are reported in the Figure 3. It is quite clear that the ASAXS curves are similar inducing a low standard errors.

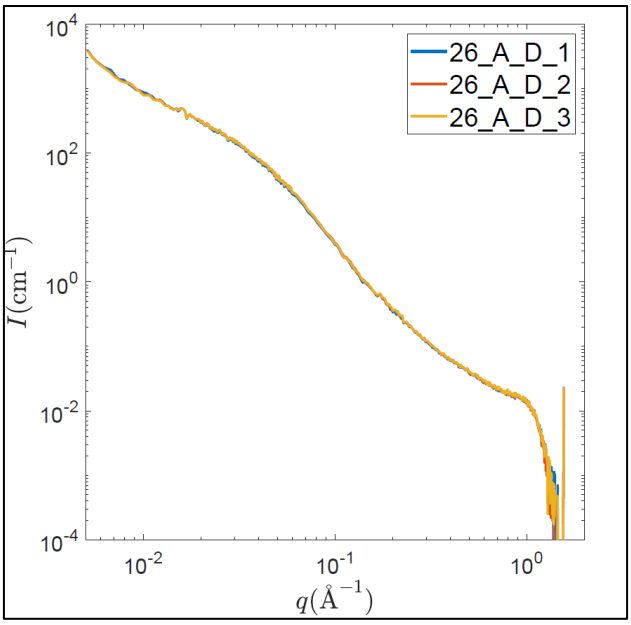

Figure 3. Reproduction of ASAXS ($I(E_3) - I(E_5)$) curves for the 26_A_D catalyst.

A nonlinear least-squares adjustment of this three ASAXS $I(E_3) - I(E_5)$ signal is performed to quantify the standard errors. Standard errors concerning the obtained parameters mentioned previously are reported in Table 2. As induced by the ASAXS $I(E_3) - I(E_5)$ curves (see Figure 3), the intrinsic standard errors are very low except for the L_{slabs} with a standard error of around 11%.

Table 2. Results obtained on the 26_A_D sample three times at the exact same point.

	L_{slabs} (nm)	S_{slabs}	C_{ag} (%)	$Absolute\ C_{ag}$ (%)	W_{ag} (nm)	L_{ag} (nm)	$\langle V_{ag} \rangle$ (nm³)	N_{ag}/V_s (10^{-6} nm^{-3})
26_A_D_1	3.2	1.0	59	15	7.5	68.4	434	1.1E-04
26_A_D_2	2.7	1.0	60	16	7.5	67.5	399	1.2E-04
26_A_D_3	3.5	1.0	60	15	7.5	67.0	451	1.1E-04
Average	3.2	1.0	59.5	15.5	7.5	67.6	428	1.1E-04
Absolute uncertainties	0.34	0.00	0.60	0.15	0.03	0.60	21.49	6.6E-06
Relative uncertainties (%)	10.9	0.0	1.0	1.0	0.5	0.9	5.0	5.9

Mention that these measurements have been carried out for a different 26_A_D capillary than the one used and presented in the main text. This can explain the slightly different results about the obtained parameters presented in the main text and the one presented in Table 2.

It is also necessary to mention that ASAXS technique is a local technique carried out on grounded catalysts placed in capillaries. If the catalyst is heterogeneous in terms of

171 macroscopic Mo distributions or support texture, a different ASAXS signal could be obtain by
172 analyzing a different position on the capillary. Using a capillary of 1.5 mm diameter makes it
173 possible to limit this phenomenon by averaging the ASAXS signal of the catalysts
174 heterogeneities.

TEM statistical analysis

In the main text, TEM results have been discussed through two parameters such the mean slabs length and the average stacking. However, it is possible to represent the MoS_2 slabs size and stacking distribution by a lognormal law. Such distributions are reported in Figure 4.

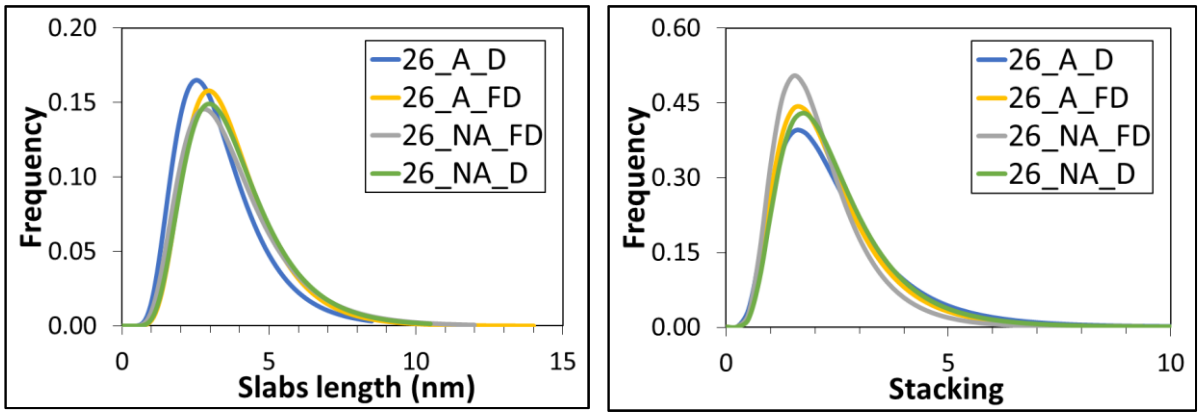

Figure 4. Slabs size distributions (mean aggregate length, left) and slabs stacking distribution (right) of the 26 wt% MoO_3 catalysts from TEM statistical analysis.

The slabs length are between 1 to 10 nm, the stacking level is around 1 to 6.

References

[1] C. T. Chantler, *Journal of Physical and Chemical Reference Data* **1995**, *24*, 71–643.

[2] C. T. Chantler, *Journal of Physical and Chemical Reference Data* **2000**, *29*, 597–1056.

[3] H.-G. Haubold, T. Vad, N. Waldöfner, H. Bönnemann, *Journal of Applied Crystallography*, *36*, 617–620.

[4] H.-G. Haubold, X. H. Wang, *Nuclear Instruments and Methods in Physics Rsearch B* **1995**, *97*.

[5] H.-G. Haubold, X. H. Wang, G. Goerigk, W. Schilling, *Journal of Applied Crystallography* **1997**, *30*, 653–658.

[6] H.-G. Haubold, X. H. Wang, H. Jungbluth, G. Goerigk, W. Schilling, *Journal of Molecular Structure* **1996**, *383*, 283–289.

[7] F. Wen et al., *Eur. J. Inorg. Chem.* **2005**, *2005*, 3625–3640.

[8] T. Binninger, M. Garganourakis, J. Han, A. Patru, E. Fabbri, O. Sereda, R. Kötz, A. Menzel, T. J. Schmidt, *Phys. Rev. Applied* **2015**, *3*.

[9] S. Humbert, G. Desjouis, T. Bizien, L. Lemaitre, A. L. Taleb, C. Dalverny, L. Sorbier, A. S. Gay, *Journal of Catalysis* **2018**, *366*, 202–212.